

Failure Precursors and Failure Mechanisms in Hierarchically Patterned Paper Sheets in Tensile and Creep Loading

Mahshid Pournajar,^{1,*} Tero Mäkinen²,^{ORCID} Seyyed Ahmad Hosseini,¹ Paolo Moretti,¹ Mikko Alava,² and Michael Zaiser¹

¹*WW8-Materials Simulation, Department of Materials Science, Friedrich-Alexander-Universität Erlangen-Nürnberg, Dr.-Mack-Str. 77, Fürth 90762, Germany*

²*Department of Applied Physics, Aalto University, P.O. Box 11100, Aalto, Espoo FI-00076, Finland*

 (Received 13 March 2023; revised 2 June 2023; accepted 14 July 2023; published 3 August 2023)

Quasibrittle materials endowed with (statistically) self-similar hierarchical microstructures show distinct failure patterns that deviate from the standard scenario of damage accumulation followed by crack nucleation and growth. Here we study the failure of paper sheets with hierarchical slice patterns as well as nonhierarchical and unpatterned reference samples, considering both uncracked samples and samples containing a macroscopic crack. Failure is studied under displacement-controlled tensile loading as well as under creep conditions. Acoustic emission records and surface strain patterns are recorded alongside stress-strain and creep curves. The measurements demonstrate that hierarchical patterning efficiently mitigates against strain localization and crack propagation. In tensile loading, this results in a significantly increased residual strength of cracked samples. Under creep conditions, for a given range of lifetimes, hierarchically patterned samples are found to sustain larger creep strains at higher stress levels; their creep curves show unusual behavior characterized by multiple creep rate minima due to the repeated arrest of emergent localization bands.

DOI: [10.1103/PhysRevApplied.20.024008](https://doi.org/10.1103/PhysRevApplied.20.024008)

I. INTRODUCTION

Hierarchically (micro)structured materials contain elements that have structure within themselves in such a manner that the system exhibits a self-similar pattern of geometrically similar features on multiple scales. A material's hierarchical order n can be defined as the number of scale levels with recognized structure. For $n = 0$, the physical properties of the material can be analyzed as those of a structureless continuum. Materials with $n = 1$ may be envisaged in terms of the arrangement of atoms or granules into ordered crystal or lattice structures [1], or into disordered cohesive assemblies. Examples of two-level material architectures include the geometrical microstructure of cellular metamaterials with regular atomic microstructure of the matrix material and well-defined periodic metastructure. Many biological materials such as nacre, bivalve shell, bone, and tendon collagen have, instead, multilevel hierarchical microstructures that extend from the nanoscale to the macroscale. Although they are made of brittle constituents, such materials may exhibit remarkable stiffness, good toughness, high strength, and low weight [2–7]. By

mimicking the hierarchical structures of biological materials, novel approaches may be sought to enhance the mechanical properties of architected (meta)materials [8].

Numerical modeling has been considered in several publications as a tool for designing hierarchical structures and predicting their properties. Simple modeling approaches such as fiber bundle models may be extended to hierarchical materials [9], but cannot adequately represent crack-tip stress concentrations that are an essential aspect in the failure of materials by crack propagation. Spatial stress concentrations and crack propagation can be described by fuse and beam network models. As an example, Moretti *et al.* [10] used a random fuse model to comparatively study failure behavior of materials with and without hierarchical microstructure. The failure behavior of hierarchical materials, as well as the resulting super-rough crack morphology, was found to differ significantly from the behavior of nonhierarchical ones. Hierarchical patterning of interfaces was also studied using fuse network models, and it was shown that hierarchical patterning delays detachment and improves interfacial adhesion [11]. Hosseini *et al.* [12] introduced a hierarchical version of a beam network model to simulate hierarchically patterned materials. The findings of these authors show that the failure of hierarchically structured materials is caused by local damage nucleation followed by damage percolation rather than

*mahshid.pournajar@fau.de

critical crack propagation, a finding which holds for both two-dimensional [12] and three-dimensional [13] structures. In both cases, crack profiles show large deflections as failure arises from the coalescence of widely separated microcracks. Zaiser *et al.* [14] not only conducted simulations but also experiments on two-dimensional quasibrittle materials loaded along a single axis. It was demonstrated that hierarchical patterning considerably increased crack propagation resistance both in terms of the peak stress and the work of failure of precracked samples.

These studies indicate that hierarchically structured materials do not fail by coherent crack propagation even when they consist of brittle elements. In materials without hierarchical structure, the applied stress is concentrated at the crack tip and damage or plasticity localize in a narrow zone around the crack tip, known as the fracture process zone (FPZ) [15]. In quasibrittle materials, such as paper, microcracks nucleate, grow, and coalesce ahead of the crack tip, creating again a fracture process zone of enhanced damage [16]. Here we demonstrate that hierarchical patterning of the material improves toughness and damage tolerance by reducing stress concentrations and significantly widening the process zone in front of the crack tip. To this end, we study paper sheets with hierarchical gap patterns created by a laser cutter, as well as reference specimens containing gaps of equal orientation and overall length in nonhierarchical random arrangement, and pristine sheets. We note that the patterned sheets can be envisaged as an extreme limit case of “calcitelike” hierarchical composites as studied by Buehler and coworkers [7, 17] where weak and compliant, lamellar inclusions are embedded into a hard and brittle matrix (in the present study the inclusions would be of zero elastic modulus as they correspond to the created gaps, whereas the matrix corresponds to the quasibrittle paper sheet).

We perform displacement-controlled tensile as well as time-dependent creep tests to investigate how hierarchical structure affects the failure mode under different loading conditions. We put edge notches of different length into the samples to induce damage localization, and we monitor damage accumulation by acoustic emission (AE) recording in conjunction with the digital image correlation (DIC) technique to extract displacement fields and spatial strain distribution. In this manner we quantitatively characterize the distinct differences in failure behavior between hierarchical and nonhierarchical samples.

II. EXPERIMENTAL PROCEDURE

A. Specimen preparation

Experiments were carried out on rectangular copy paper sheets of thickness $t = 0.1$ mm with a weight of 80 g/m², which were tested under uniaxial loading conditions with loads acting parallel to two of the sides of the sheets. The loading direction was taken parallel to the machine

direction of the paper manufacturing process, leading to enhanced strength and reduced ductility of the pristine sheets relative to the perpendicular “cross” direction. Following the usual geometry of a tensile testing apparatus, the loading direction is henceforth referred to as the vertical direction. We used sheets of dimensions $210 \times 150 \times 0.1$ mm³ as well as $105 \times 75 \times 0.1$ mm³. For the larger samples, two stripes of 30 mm width at the top and bottom edges of the sample were placed in the clamps; for the smaller samples, the width of these stripes was 15 mm; these stripes were left unpatterned. On the central part of the samples, of dimensions $L \times L \times t$, where $L = 150$ mm for the larger and $L = 75$ mm for the smaller samples, patterns of load-parallel (vertical) cuts were created using a laser cutter (model Sculpfun S9).

Different types of deterministic and stochastic, hierarchical and nonhierarchical cut patterns were created. We first explain the construction method underlying a deterministic hierarchical pattern (DHP). A top-down construction of a four-level DHP pattern is illustrated in Fig. 1(a). The green dashed lines indicate the upper and lower edges used for clamping; the space between these lines is denoted as a level-1 load-carrying module of size L . Next, two central load-parallel cuts are applied to divide this space into four level-2 modules; horizontally, a remaining ligament of thickness $t_c = 1$ mm between the cuts provides a lateral connection that spans the system in the horizontal direction (central dashed line at level 2). The load-parallel cuts are illustrated as blue lines, and the red dashed lines illustrate lateral connections between modules. At level 2, each of the four modules is again divided by two central cuts into four level-3 modules, with a horizontal lateral connection of thickness $t_c = 1$ mm spanning the modules, and after that, each of the 16 level-3 modules is again subdivided by two shorter cuts into four modules with one lateral connection to produce a total of 64 level-4 modules. This process is continued for up to $n = 7$ levels; the ensuing pattern consists of $N_s = 2^{n-1}$ stripes of paper of width $w_s = L/2^{n-1}$ partly separated by cuts. In this pattern, both the lengths of load-parallel cuts and the lengths of lateral connections obey power-law statistics [10].

In addition to the DHP, we also generate a randomized version named the shuffled hierarchical pattern (SHP). To this end, we envisage the DHP pattern as a square block divided into $2N_s - 1$ vertical slabs [two of them are marked in red in Fig. 1(b), left]. The thickness of these slabs is $w_s/2$. Along N_s of these slabs, the paper is fully connected, whereas along the remaining $N_s - 1$ slabs, cuts of varying length alternate with discrete lateral connectors of width t_c . We now randomly shuffle the vertical slabs to create a randomized structure of the same size and total cut length. Next, we envisage the ensuing pattern as a stack of $2N_s - 1$ horizontal slabs of thickness $w_s/2$ [two of these are marked in green in Fig. 1(b), left] and randomly shuffle the horizontal slabs. As discussed elsewhere [10, 13], this

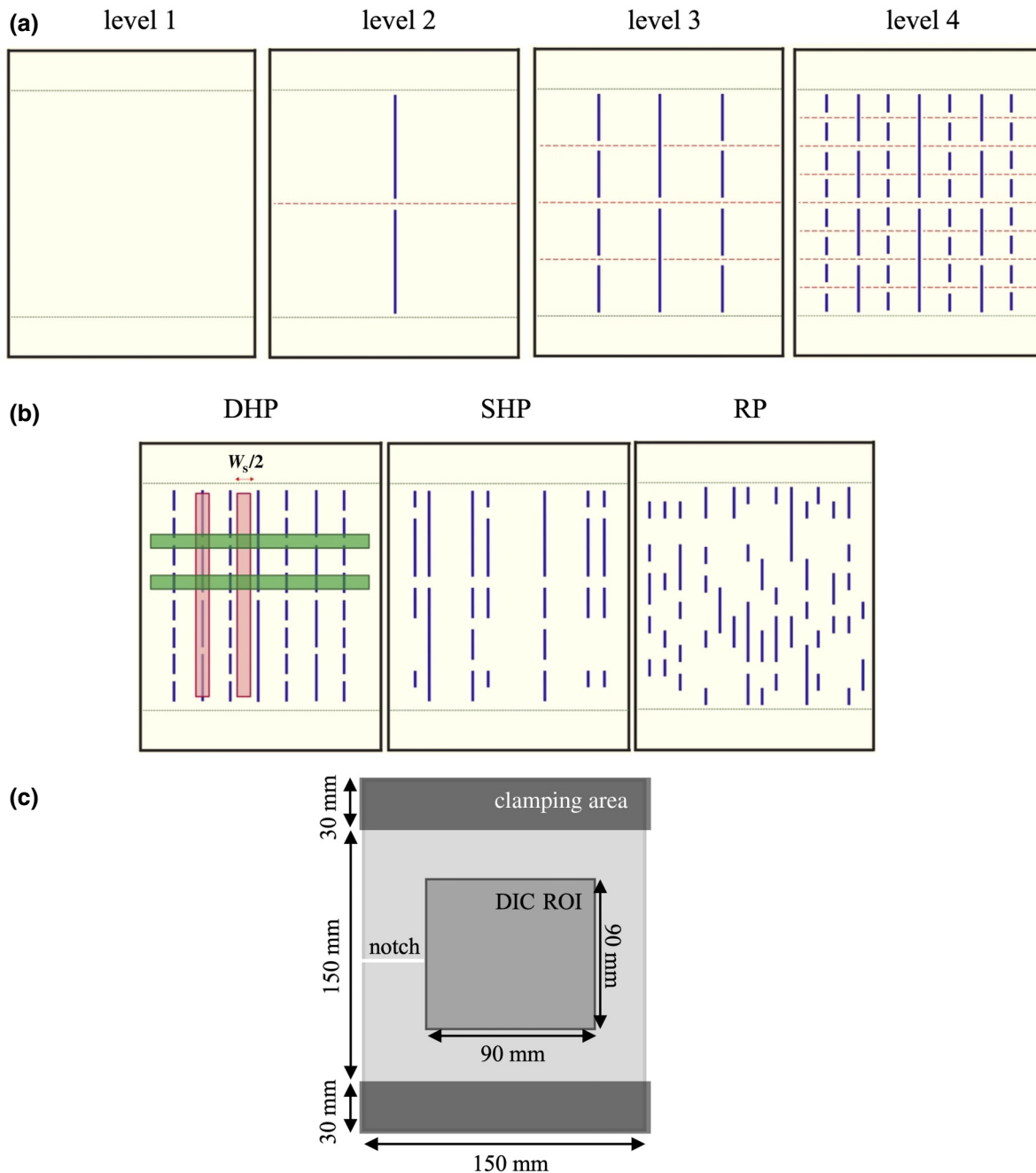


FIG. 1. (a) Top-down construction of a four-level deterministic hierarchical pattern (DHP) of cuts. First, we select a paper sheet with dimensions $210 \times 150 \times 0.1 \text{ mm}^3$, allocating stripes of thickness 30 mm at the top and bottom for clamping (level 1). Next, the paper is divided into four modules by two load-parallel (vertical) cuts along the centerline of the sample with 1-mm space between them (level 2); here the blue lines are the cuts that have a thickness of 0.1 mm, and the red dashed lines indicate the connectors between them in the load-perpendicular direction. Next, each of the four modules is again divided by two shorter central cuts into four modules with one module-spanning connection (level 3), and after that each of the 16 modules is again subdivided by two shorter cuts into four modules (level 4). (b) Four-level DHP structure together with structures with shuffled hierarchical pattern (SHP) and random pattern (RP), illustrating the patterns of cuts for the different structures. (c) A paper sheet with dimensions $210 \times 150 \times 0.1 \text{ mm}^3$, allocating 30-mm stripes at the top and bottom for clamping, with a central side notch on the left edge and having a DIC region of interest of $90 \times 90 \text{ mm}^2$.

randomization leaves the total cut length unchanged. It also preserves the power-law length statistics of load-parallel cuts and of lateral connectors, which is constitutive for a hierarchical pattern.

We also generated random patterns (RPs) to match the DHP and SHP patterns. A random pattern matching the above described hierarchical patterns again consists of a sheet of paper divided into $2N_s - 1$ vertical slabs as in

the SHP construction. Along the vertical centerlines of the slabs, cuts are now applied randomly such that the sum of all cut lengths is the same as in the matching hierarchical patterns, as is the minimum spacing t_c between two vertically adjacent cuts and the minimum cut length $l_c = w_s - t_c$. However, now the cut endpoints are located randomly on the divider lines under the constraints of minimum spacing $t_c = 1$ mm, minimum cut length, and zero overlap of cuts. This leads to an exponential distribution of cut lengths. A four-level DHP structure as well as corresponding SHP and RP structures are illustrated in Fig. 1(b). DHP and SHP samples representing seven-level and six-level structures were used in this work. Paper without any pattern (NP) was also used for comparison.

In order to investigate flaw sensitivity of failure properties, samples in the as-patterned state were tested alongside samples containing single load-perpendicular side notches, akin to macroscopic mode-I cracks. Notches with different lengths a ranging from 0 to 0.6 of the specimen width L were cut in the load-perpendicular direction, starting from the left side of the samples. The notches were vertically located at random positions between 0.25 and 0.75 of the sheet length.

B. Testing and characterization

An Instron Electropuls E1000 tensile testing machine was used in all tests. Uniaxial displacement-controlled tensile tests were done at a displacement rate of 0.05 mm/s. The sample was fixed between two clamps; the upper clamp and grip were movable while the lower one was stationary. All tests were carried out at room temperature.

On samples of size $210 \times 150 \times 0.1$ mm³ with side notches of length $a = 30$ mm, creep tests also were performed. For such samples, the average peak load in a displacement-controlled tensile test was determined to be 265 N for SHP and DHP samples, and 210 N for RP and NP samples. In creep testing, the load was increased at a constant rate within 5 s to 85% of the tensile peak load of the respective type of notched patterned sheet (DHP, SHP, RP, and NP), and then kept constant. Because of the wide scatter of sample lifetimes, a window of lifetimes ranging from 6 to 300 s was imposed and samples that did not fail within this time window were discarded.

Displacement fields were evaluated using a contactless technique called digital image correlation (DIC) [18]. DIC measurements were performed on samples of size $210 \times 150 \times 0.1$ mm³ with side notches of length $a = 30$ mm. A camera recorded high-resolution images (0.25 mm/pixel) of the sample at a rate of one image per second during the total test time from the beginning of the loading until the final failure. Two LED lamps were positioned on both sides of the samples to adjust the light on the surface of the sample. To provide grayscale contrast, a speckle pattern was printed on the specimens. DIC was carried out using

Ncorr software [19]. In DIC, a reference image is chosen at the beginning of the loading. A region of interest (ROI) is specified on the reference image, which was taken to be an area of 90×90 mm² in front of the crack tip; see the color-scale area in Fig. 2 below. Figure 1(c) illustrates the total dimensions of the paper samples and the location of the region of interest.

The ROI is then partitioned into (overlapping) circular subsets, i.e., groups of points over which deformation is assumed to be homogeneous, with center points placed at each pixel in the ROI. To track the displacement of these subsets, DIC tries to find a deformation function that optimally maps the pattern of the reference image onto the pattern of the current test image at time t . In our analysis, a subset radius of 16 pixels (corresponding to 4 mm) was used, which was found to provide a reasonable compromise between too noisy displacement data (too small subset size) and decreased accuracy caused by the smoothing effect of large subsets [20]. The sum of squared differences correlation criterion is used to analyze the similarity between elements in the reference and target images [21]. The displacement of a point at (x, y) in the reference image is given by a vector $\mathbf{u} = (u, v)$ and the vertical Green-Lagrange strain used is calculated as

$$\epsilon_{yy} = \frac{\partial v}{\partial y} + \frac{1}{2} \left[\left(\frac{\partial u}{\partial y} \right)^2 + \left(\frac{\partial v}{\partial y} \right)^2 \right], \quad (1)$$

where the partial derivatives are inferred by locally fitting a plane of radius three pixels (0.75 mm) to the displacement field [19].

The AE system consisted of a piezoelectric transducer and a rectifying amplifier, an analog-to-digital converter, and a computer. The piezoelectric transducer was gently attached directly to the back side of the paper. The transducer was in direct contact with the paper to avoid the requirement for excessive amplification. The AE signal was acquired at an acquisition frequency of 100 kHz during the time of recording stress-strain curves in uniaxial tensile tests and strain-time curves in creep tests. For each type of test and each sample type, AE recordings of 20 samples were taken.

Acoustic emission signals from deformed paper samples are characterized by an intermittent sequence of discrete AE bursts [22]. To analyze statistical signatures of this “crackling noise” [23] signal, the acquired signals were postprocessed by transforming them into discrete events using an amplitude threshold A_{th} , defining an event as the compact time interval Δt_i between sequential upward and downward crossings of the threshold and denoting the time of the upward crossing as the event starting time t_i . The threshold is adjusted to separate bursts from background noise, using the fact that, for varying A_{th} , the total event number $N(A_{th})$ exhibits two distinct regimes, depending

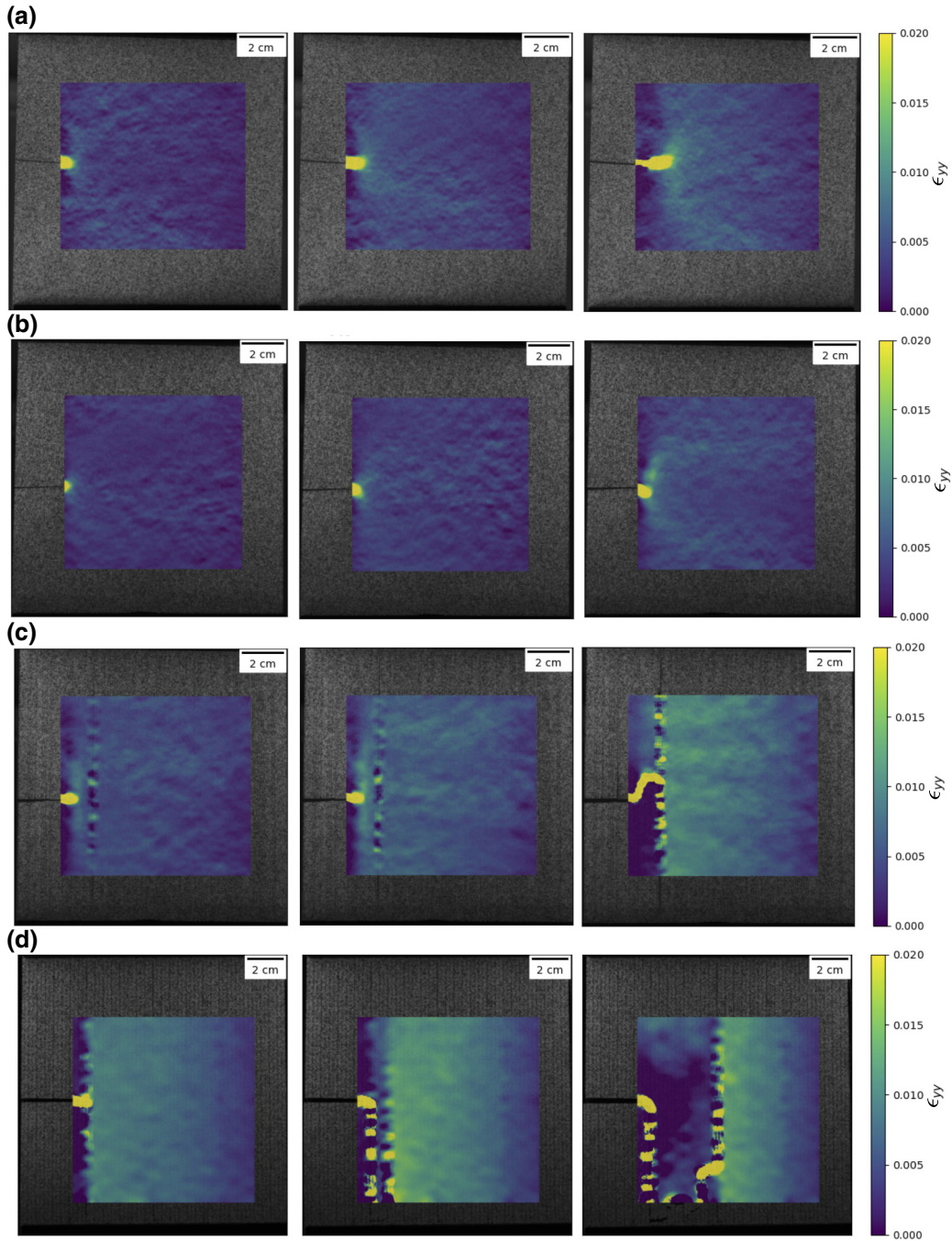


FIG. 2. DIC maps of the load-parallel strain component ϵ_{yy} in displacement-controlled tensile tests for displacement levels $\epsilon/\epsilon_f = 0.6$ (left), 0.75 (center), 0.9 (right). Samples with four different cut patterns are shown: (a) no pattern (NP), (b) RP, (c) SHP, (d) DHP. All samples have a size of $150 \times 150 \text{ mm}^2$ with a central side notch of length $a = L/5 = 30 \text{ mm}$ on the left edge. Strain is shown in color scale over a region of interest of $90 \times 90 \text{ mm}^2$; the rest of the samples are shown in grayscale.

on whether it is dominated by the discrete bursts or the continuous background noise.

For each event, the integral of the squared acoustic amplitude $A(t)$ over the event duration was used to calculate the event energy E_i ,

$$E_i = \int_{\Delta t_i} A^2(t) dt. \quad (2)$$

A set of energy-time pairs $(t_1, E_1), \dots, (t_n, E_n)$ characterizes the resulting sequence of discrete events. Acoustic event energies $P(E)$ were found to be distributed according to a power law, $P(E) \propto E^{-\beta}$, and the value of the exponent β was estimated using the method of maximum likelihood [24]. This method is based on identifying a β value that maximizes the likelihood function. First the

original data, here energy values, are restricted between a lower cutoff E_{low} and an upper higher cutoff E_{up} . By changing these two values, a map of exponent values can be obtained. By discarding areas where the error estimate of the maximum-likelihood estimate exceeds a prescribed level (here 0.10), an error margin can be set for the exponent (here $\delta\beta = 0.05$). One then identifies the largest area of the map corresponding to $\beta \pm \delta\beta$ and takes this as the estimated β value (as well as the corresponding extremal E_{low} and E_{up} values as the limits of the power-law fit) [25].

III. RESULTS

A. Displacement-controlled tensile test

We first focus on the effects of patterning on the distribution of strain in tensile testing of notched samples, considering DHP, SHP, RP, and NP samples with a common notch length of 30 mm. Figure 2 illustrates snapshots of the spatial strain patterns of hierarchical and nonhierarchical samples at 60%, 75%, and 90% of the tensile failure strain ε_f . The color scale in these snapshots indicates the local strain in the loading direction. While notched RP and NP specimens exhibit strain concentrations ahead of the crack tip, indicating the presence of a localized fracture process zone, no such strain localization can be seen in hierarchical DHP and SHP samples. At the same time, the overall strain level supported by the hierarchical samples is much higher. The empirical findings were compared with results of simulations based on two-dimensional (2D) beam network models. These simulations consider the same types of structures and the same notch geometry and loading mode as the experiments in Fig. 2. The simulation methodology has been described in detail elsewhere [12]; we refer the reader to this paper for details. Strain patterns in simulation and experiment are in good qualitative agreement, as shown in Fig. 3 for the patterns observed at the peak stress of hierarchical DHP and nonhierarchical RP samples. The RP samples in both simulation and experiment exhibit a distinct region of high strain around the crack tip, while in DHP samples no discernable crack-tip strain concentration can be found. Accordingly, the crack propagation modes are quite different: in the nonhierarchical samples, fracture occurs by crack propagation driven by high stresses near the crack tip. In hierarchical samples, on the other hand, the hierarchical gap pattern reduces stress concentrations and impedes crack propagation, leading to early deflection of the crack and diffuse damage accumulation across the entire sample. As a result, DHP and SHP samples can absorb significantly more energy and sustain larger deformation before failing. Indeed, in DHP samples the local strain in the intact ligament ahead of the crack may reach levels comparable to the failure strain ε_f^0 of an uncracked sample, demonstrating the efficiency of hierarchical patterns in mitigating the strength deterioration due to the preexisting crack.

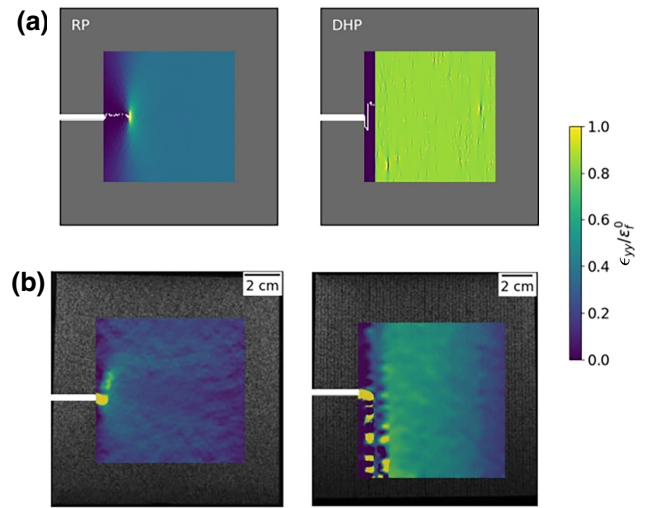


FIG. 3. Comparison of strain patterns in simulation (a) and experiment (b) for the nonhierarchical (RP; left) and hierarchical (DHP; right) samples. Strain patterns are determined at the peak stress in a displacement-controlled test, with the initial crack of length $a/L = 0.2$ marked in white. The color scale indicates the local strain, normalized by the mean failure strain ε_f^0 of a DHP sample without an initial crack.

Acoustic emission allows us to monitor the temporal accumulation of damage. Since AE in paper proceeds in the form of a sequence of intermittent events, we consider the statistics of AE event energies and compare results for hierarchical and nonhierarchical samples. Figure 4 depicts the probability density function $P(E)$ of event energies for NP, RP, SHP, and DHP samples in displacement-controlled tensile tests. The probability density function of acoustic event energies follows a power law, $P(E) \propto E^{-\beta}$ for around six decades, with β values ranging from 1.4 to 1.6. Power-law distributions with exponents in this range were observed in samples both with and without an initial notch [26], e.g., in tensile tests of notched paper, a value of $\beta \sim 1.4 \pm 0.1$ was determined by Rosti *et al.* [27]. Here we study avalanche statistics in hierarchically patterned samples and find stable exponent values $\beta \sim 1.5 \pm 0.05$, without statistically significant differences between hierarchical and nonhierarchical samples, as shown in Fig. 4. We note that the upper limits of the maximum likelihood fits coincide with the largest event sizes in the respective statistical samples, indicating that there is no intrinsic upper cutoff to the event size. The size of the largest events is somewhat higher in hierarchical than in nonhierarchical samples.

The total number of acoustic emission events observed in all 20 experiments during the tensile test is 10 287, 5208, 6269, and 5837 for NP, RP, SHP, and DHP, respectively. Hence, NP samples seem to exhibit more AE events than patterned samples. This may however be an artefact of the recording method: the cuts in the patterned paper sheets

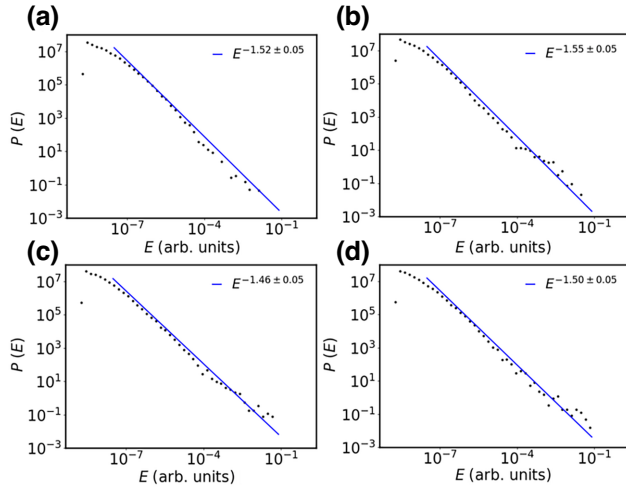


FIG. 4. Probability density function of event energies as determined from 20 displacement-controlled tensile tests. (a) NP, (b) RP, (c) SHP and (d) DHP paper sheets. The sample between the clamps is of size $150 \times 150 \text{ mm}^2$ with a side notch of length $a = L/5 = 30 \text{ mm}$. The blue lines correspond to the power-law fits given in the figure legends.

lead to a less perfect contact between the transducer and the paper sheet and at the same time impede acoustic wave transmission, thus reducing the sensitivity of the transducer in recording the sample's released acoustic emission energy.

B. Fracture mechanical size effect

In fracture mechanics of quasibrittle materials, the peak stress σ_p sustained in a tensile test by a sample containing a mode-I crack decreases with increasing crack length a . The relationship between peak stress and crack length can, in generalization of Griffith's theory, be written as

$$\sigma_p = \frac{K_{Ic}}{\sqrt{\pi(a + a_0)}} f\left(\frac{a}{L}\right). \quad (3)$$

This equation takes into account the fact that in the limit of vanishing crack length, strength must converge to a finite value; the characteristic length a_0 can be interpreted as the characteristic size of the fracture process zone (see, e.g., Ref. [28]). Function $f(a/L)$ accounts for effects of sample size L and sample geometry; for geometrically similar samples (fixed a/L), this function reduces to a constant. For hierarchical samples, an alternative relationship has been proposed [14] based on the idea that, in such samples, stress concentrations are completely absent such that the strength of a notched sample is simply the strength $\sigma_{p,0}$ of an un-notched sample, corrected by the cross-section reduction due to the initial notch:

$$\sigma_p = \sigma_{p,0} \left(1 - \frac{a}{L}\right). \quad (4)$$

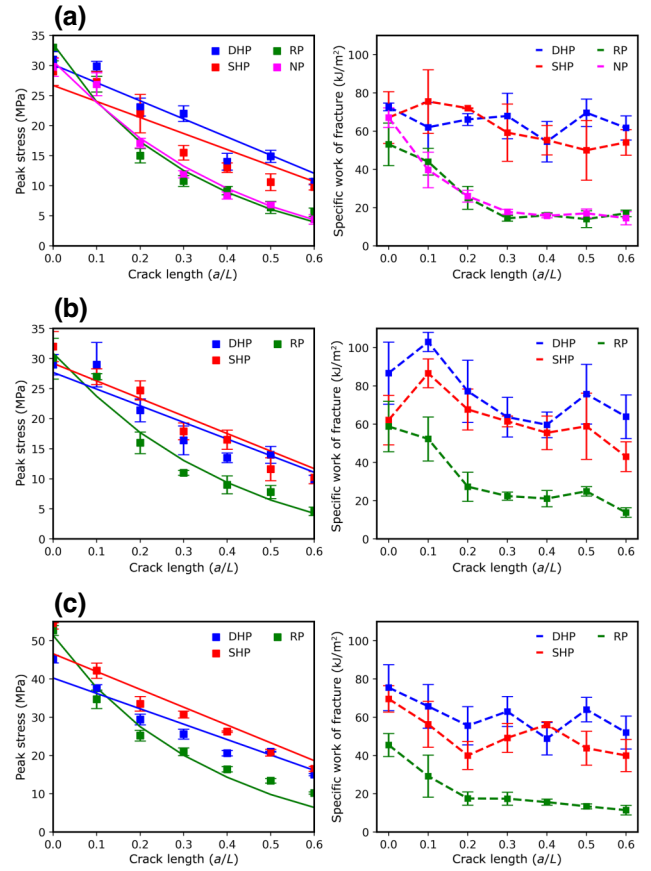


FIG. 5. Left: peak stress as a function of the notch length. Right: specific work of fracture as a function of the notch length for NP, RP, SHP, and DHP paper sheets in displacement-controlled tensile tests. Sample size L and the number of hierarchy levels n are varied from top to bottom: (a) $L = 150 \text{ mm}$, $n = 7$; (b) $L = 150 \text{ mm}$, $n = 6$; (c) $L = 75 \text{ mm}$, $n = 6$.

To investigate how the alternative size effect descriptions apply to hierarchical and nonhierarchical samples, we have plotted the peak stress of square samples containing a side notch as a function of notch length a . Different combinations of sample size L ($L = 75, 150 \text{ mm}$) and the number of hierarchy levels n ($n = 6, 7$) were considered, using both NP, RP, DHP, and SHP samples; RP samples were matched to the hierarchical samples by using a similar value of the spacing $w_s = L/2^{n-1}$ between vertical cuts. Results are shown in Fig. 5 (left). The data were fitted by both Eqs. (3) and (4), where, for f , a relationship given by Tada [29] for a single-edge notch specimen was used: $f^{-1}(x) \approx 1.122 + 0.231x + 10.55x^2 - 21.710x^3 + 30.382x^4$. Resulting fit parameters are presented in Table I alongside values of the coefficient of determination R^2 that serves as a measure of the quality of fit.

For nonhierarchical NP and RP samples, Eq. (3) yields a consistently better description than Eq. (4), whereas for

TABLE I. Summary of fitting parameters for different samples using Eqs. (3) and (4).

Sample	R^2 [Eq. (3)]	a_0 (mm)	K_{Ic} (MPa m ^{1/2})	R^2 [Eq. (4)]	$\sigma_{P,0}$ (MPa)
NP-L150-N7	0.97	31.05	27.77	0.7	23.2
RP-L150-N7	0.97	19.8	24.24	0.65	23.6
RP-L150-N6	0.96	28.95	26.9	0.69	23.16
RP-L75-N6	0.96	11.25	39.5	0.71	37.57
SHP-L150-N7	0.95	222	69.8	0.88	26.69
SHP-L150-N6	0.96	801	139.7	0.92	29.21
SHP-L75-N6	0.90	254	178.7	0.91	46.5
DHP-L150-N7	0.93	2×10^7	23 650	0.92	30.16
DHP-L150-N6	0.91	1129	156.6	0.88	27.69
DHP-L75-N6	0.88	9000	897	0.91	40.2

SHP and DHP samples, Eqs. (3) and (4) provide a comparable quality of fit. Upon closer inspection of the fit parameters, it is however evident that the parameters obtained for hierarchical samples with Eq. (3) are unphysical: in all cases, the fitted values of the process zone size exceed the sample size, which implies that a description in terms of fracture mechanics is unfeasible and the obtained fracture toughness values are physically meaningless. We note that fracture testing standards such as ASTM E399 impose the requirement that all relevant dimensions—specimen size, ligament size, crack length—must be reasonable multiples of the estimated process zone size. This condition is for the hierarchical samples grossly violated. In our nonhierarchical samples, on the other hand, the condition of a sufficiently small process zone size turns out to be approximately valid. Accordingly, the fit curves shown in Fig. 5 (left) represent fits of Eq. (3) for nonhierarchical RP and NP samples, and fits of Eq. (4) for hierarchical SHP and DHP samples.

The above qualitative observations hold for all investigated samples irrespective of sample size and the number of hierarchy levels. Comparison of Figs. 5(a) and 5(b) also indicates that strength does not depend strongly on the number of hierarchy levels. At the same time, we note that the strength of samples increases with decreasing sample size, as shown by comparing Figs. 5(b) and 5(c). The failure strength of samples without cracks is around 50 MPa for $L = 75$ mm and 30 MPa for $L = 150$ mm (see Fig. 5). Such sample-size dependence of the strength in unnotched samples is an example of the typical statistical size effects found in disordered materials, where crack nucleation is controlled by the weakest spots of the disordered microstructure—minima of strength that are, on average, lower in bigger samples [30]. We also observe that, in samples containing an initial notch, smaller samples show higher strength for the same a/L value. This is entirely in line with the classical fracture mechanical size effect: for a given a/L value, the crack length a in the $L = 75$ mm

sample is a factor 2 smaller than in the $L = 150$ mm sample, and following Eq. (3), the peak stress is accordingly higher. The values of the a_0 parameter are, in the cases in which Eq. (3) is applicable, quite large compared to the case of ordinary paper, where one would expect 2 mm.

Figure 5 (right) shows the specific work of fracture w_f , defined as the ratio of the area under the stress-strain curve divided by the area $t(L - a)$ of the intact ligament. In RP samples, regardless of pattern level and specimen size, w_f initially decreases with crack length and then stabilizes when the crack length reaches about twice the process zone size. In hierarchical DHP and SHP samples, w_f is within the statistical scatter of the data, independent of crack length and, for long cracks, a factor of 3–4 higher than in the nonhierarchical RP and NP counterparts. As discussed in Ref. [13], this behavior can be attributed to the fact that the work of fracture is not controlled by the work needed to grow a system-spanning crack (“essential work of fracture”), but by the work expended to create diffuse damage throughout the sample (“nonessential work of fracture”) at locations that do not relate to the preexisting edge crack. This difference in failure mode is also manifest in the morphology of the fracture paths, as depicted in Fig. 6: irrespective of loading mode (displacement-controlled tensile or creep test), the hierarchical samples exhibit a super-rough crack surface, which is reminiscent of the simulated fracture patterns of hierarchical structures under tensile testing [13,14] and arises from the coalescence of microcracks disseminated along the entire length of the sample, whose system-spanning coalescence is facilitated by the widely varying length of the power-law-distributed vertical cuts. In nonhierarchical NP and RP samples, on the other hand, the fracture surface exhibits a self-affine morphology typical of disordered quasibrittle materials where failure is governed by crack growth, which is in turn controlled by the interplay of local strength fluctuations and crack-tip stress concentrations [31].

C. Creep tests

For creep testing, we used DHP, SHP, RP, and NP samples of size 150×150 mm² with a 30-mm side notch. These samples were subject to a constant, subcritical stress; the stress level σ_c was in each case taken to be 85% of the mean peak stress of the respective sample type in a tensile test. Creep lifetimes show a very significant scatter; the chosen stress level corresponds to typical creep lifetimes t_c in the range $5 \leq t_c \leq 300$ s. Samples with creep lifetimes outside this range were discarded for pragmatic reasons.

Figure 7 shows the creep strain versus the normalized creep time t/t_c for DHP, SHP, RP, and NP samples. The first 5 s of a test define the stress ramping time needed to impose the stress σ_c . The ramping time is not shown in the plots, and the strain accrued during this time appears

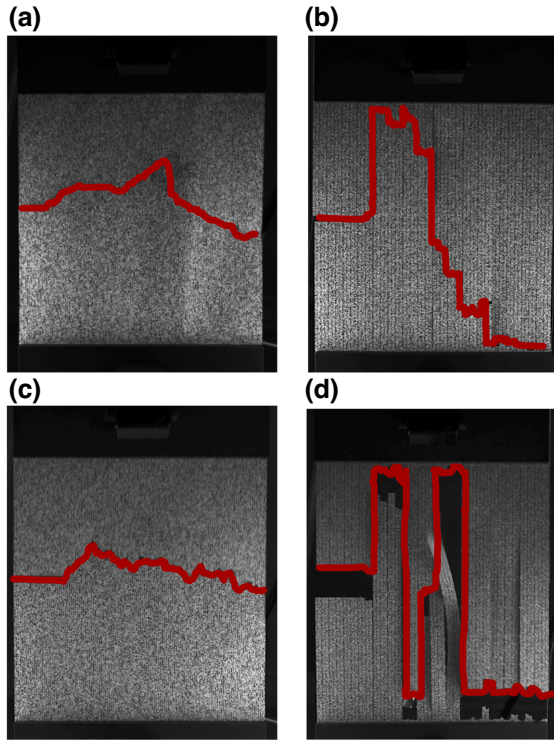


FIG. 6. Notched paper sheets after fracture in the displacement-controlled tensile test for (a) RP and (b) DHP samples and after the creep test for (c) RP and (d) DHP samples. Sample size $L = 150$ mm and notch length $a = 30$ mm.

as an instantaneous creep strain that defines the initial strain level at the onset of the creep curve. The DHP and SHP structures deform under higher stress; they show an approximately 3 times higher instantaneous strain as well as a higher overall creep strain as compared to the NP and RP samples, as shown in Fig. 7. NP and RP samples exhibit typical three-stage creep curves characterized by a decelerating primary creep stage (stage I) followed by a stage of approximately constant creep rate (stage II) and an accelerating creep stage in the run-up to failure (stage III). The distribution of the creep times or their histogram is relatively wide in all cases. The statistics we have at hand do not allow us to make any definite conclusions, but a qualitative comparison with the data of Ref. [32] and the rather exponential-like lifetime distribution found there can be made, recalling the different experimental parameters (load ratio, sample size) leading to a larger average lifetime. The three hierarchical cases resemble each other, but all also exhibit a few samples with short lifetimes, whereas the NP case has less variation. This difference results as we discuss next from varying mechanisms for crack growth resistance.

By contrast, hierarchical structures, specifically the SHP, show multistage creep curves characterized by an extended stage of primary creep interspersed with sudden strain bursts. This is most evident in Fig. 8, which

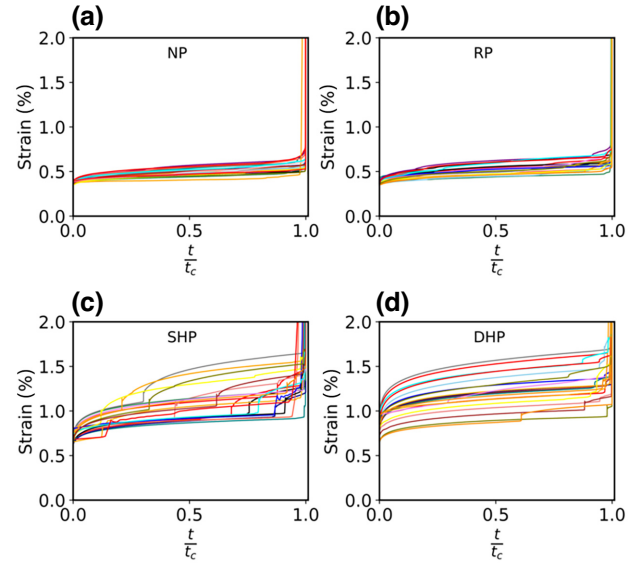


FIG. 7. Creep strain-time curves under 85% of peak load for (a) NP, (b) RP, (c) SHP, and (d) DHP samples. Each plot shows the results of 20 tested samples of size $L = 150$ mm with an initial side notch of length $a = L/5 = 30$ mm.

shows the time evolutions of the creep strain rates of DHP, SHP, RP, and NP samples after the initial ramping. In the primary creep stage, the strain rate $\dot{\epsilon}_t$ decreases according to a power law typical of so-called Andrade creep, $\dot{\epsilon}_t \propto t^{-\alpha}$. The Andrade exponent depends on the type of structure: whereas nonhierarchical structures exhibit α values close to the classical value of $2/3$ ($\alpha = 0.68$ for NP and 0.7 for RP structures), which is consistent with previously reported results for paper [33], hierarchical structures

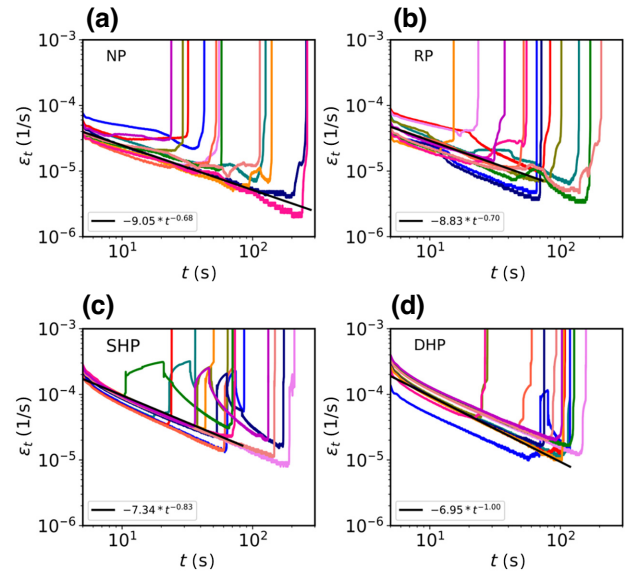


FIG. 8. Creep rate versus time curves for (a) NP, (b) RP, (c) SHP, and (d) DHP samples. Parameters as in Fig. 7.

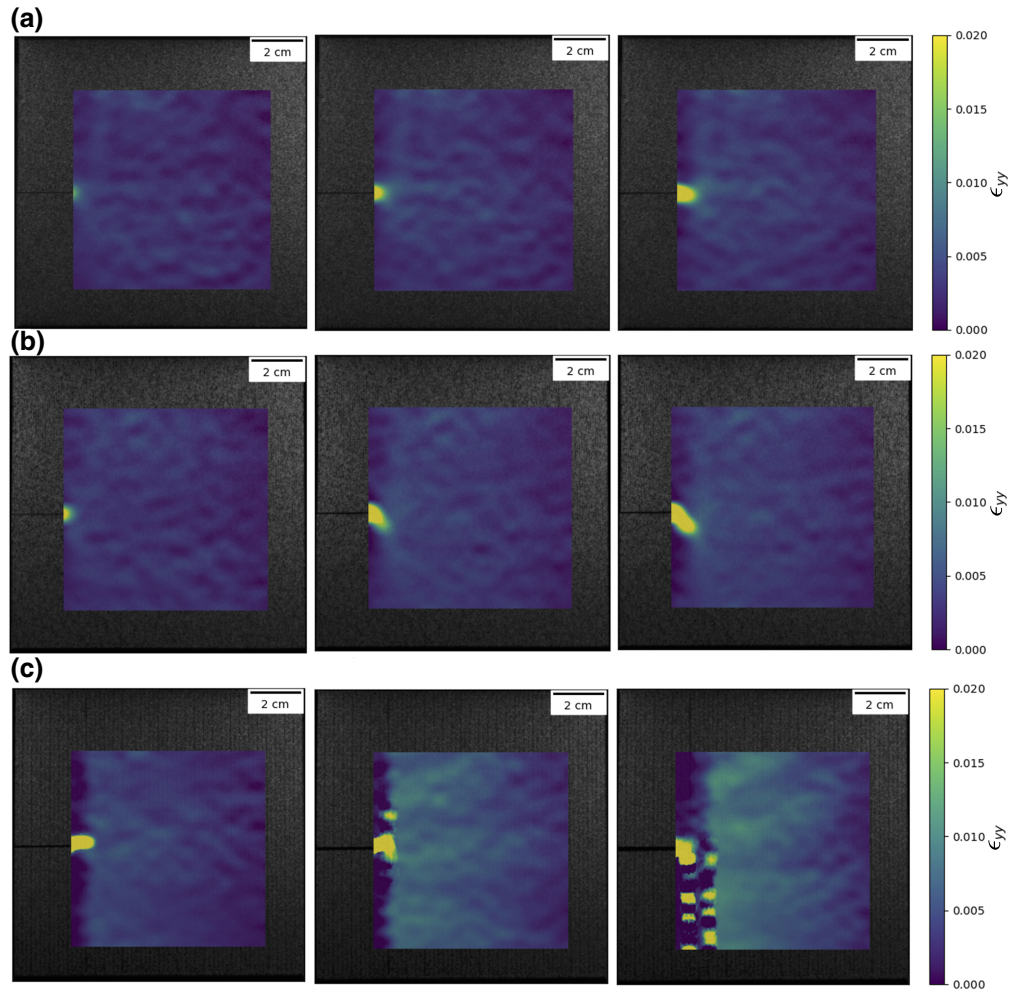


FIG. 9. Axial strain ϵ_{yy} map after ramping (left), during a steady-state step (center), during creep rate acceleration (right) before final failure in a creep test: (a) NP, (b) RP, and (c) DHP samples. Sample geometry as in Fig. 7; the color-scale region of interest is of size $90 \times 90 \text{ mm}^2$.

show higher exponents ($\alpha = 0.83$ for SHP and 1 for DHP structures). The secondary creep stage in nonhierarchical samples corresponds to a plateau of the strain rate or to a broad, sometimes fluctuating strain rate minimum. In hierarchical samples, on the other hand, the power-law decrease of the strain rate continues until global strain rate acceleration leads to final failure [34,35], but this decrease may be interspersed with sudden strain rate bursts followed by more rapid strain rate relaxation. In view of the fracture surface morphology, which shows the same features as in tensile testing (Fig. 6) and from comparison with simulations (see Ref. [12]), we may conjecture that this behavior may be associated with the arrest of the initial crack and activation of new cracks at weak spots elsewhere in the sample. This viewpoint is supported by local strain maps obtained by DIC analysis of images taken during the creep test (see Fig. 9). While NP and RP samples show strong strain localization in a pronounced FPZ around the crack tip, the DHP sample shows a much higher overall

strain level that is approximately homogeneous across the entire sample and corresponds to a high level of stress everywhere, with a concomitant propensity to distributed damage nucleation.

AE measurements were taken during the creep tests to monitor the time evolution of the creep damage. As in tensile testing, the AE signals consist of an intermittent sequence of discrete events (AE bursts). Histograms $P(E)$ of the acoustic event energies are shown in Fig. 10 for DHP, SHP, RP, and NP samples. Again, we observe for around six decades power-law behavior where $P(E) \propto E^{-\beta}$ with exponents β that turn out to be similar to the characteristic exponents of AE energy distributions reported in the literature, which were found to lie in the range $1.2 < \beta < 1.8$ in creep tests of pristine paper [22,36]. Maximum likelihood fits result in exponents $\beta = 1.75, 1.61, 1.42,$ and 1.41 for NP, RP, SHP, and DHP structures, respectively, with no apparent cutoff at large event energies. Hence, the AE exponents are slightly lower in

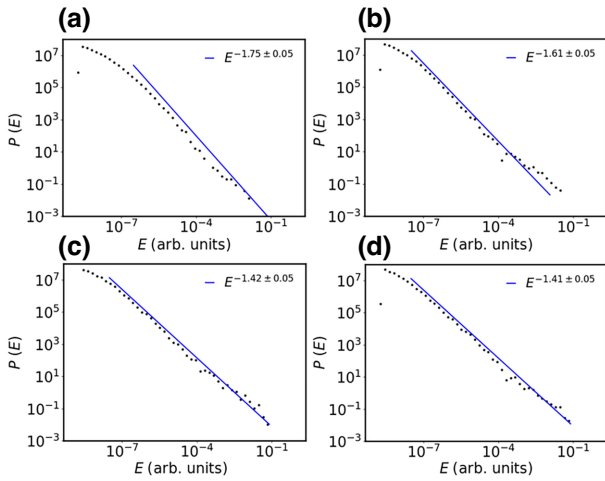


FIG. 10. Probability density function of event energies for 20 experiments in a creep test. (a) NP, (b) RP, (c) SHP, and (d) DHP paper sheets. The sample between the clamps is of size $150 \times 150 \text{ mm}^2$ with side notch of length $a = L/5 = 30 \text{ mm}$.

creep testing of hierarchical structures, as are the total event numbers, which amount to $N_{\text{ev}} = 18\,534, 8150, 4429,$ and 4518 for NP, RP, SHP and DHP structures, respectively. Again, the sizes of the largest events are higher in the hierarchical structures, reflecting the higher importance of crack nucleation as opposed to incremental crack growth.

IV. DISCUSSION AND CONCLUSIONS

We have conducted a comprehensive investigation of the failure behavior of hierarchically and nonhierarchically patterned paper sheets, using DIC and AE in conjunction with tensile and creep testing to determine the spatial and temporal characteristics of damage accumulation in the run-up to failure. Consistent with previous work on tensile deformation that comprises simulation studies [12,13] and experiments on paper and polystyrene sheets [14], we find significant differences between the failure modes of hierarchical and nonhierarchical samples that are found to hold irrespective of the testing mode (displacement-controlled tensile versus creep testing), sample size, and the number of hierarchy levels. The fact that experiments on polystyrene sheets produced results that are in qualitative agreement with those reported here for paper indicates that the beneficial effect of the hierarchical structure on damage tolerance is not specific to paper but may represent a feature that is generic to a wider range of quasibrittle materials.

Failure of nonhierarchical samples is governed by the paradigm of quasibrittle fracture mechanics; failure of such samples occurs by crack nucleation and propagation or by propagation of a preexisting crack. Fracture is driven by crack-tip stress concentrations that lead to strain

localization in a fracture process zone around the crack tip. As a consequence, the crack size dependence of strength can be well described by fracture mechanics relations with corrections for the finite process zone size.

Failure of hierarchical samples, on the other hand, defies a description in terms of classical fracture mechanics. Attempts to describe the dependency of residual strength on crack length in terms of fracture mechanics lead to internal contradiction as the mathematical fitting procedure results in process zone sizes that exceed the physical size of the sample, in line with the conjecture that structural hierarchy provides a means of shifting the process zone size across several interested hierarchical levels from the elementary to the sample scale [37,38]. On the other hand, a surprisingly good description of the phenomenology is obtained with the naive assumption that, in hierarchical samples, stress-strain concentrations are absent or at least irrelevant. This idea is supported by the findings of simulations as well as by DIC imaging that shows little or no correlation between strain pattern and crack-tip location in hierarchical samples.

While there are distinct differences in failure mode, there are also similarities between hierarchical and nonhierarchical samples. In both cases, AE signals are composed of a series of discrete events with power-law distribution of the AE event energies. In both cases, no cutoff can be discerned at large event sizes, and there are only weak differences in the energy exponents, although there is a tendency for hierarchical samples to show a lower total event number but larger values for the largest AE event energies. The insensitivity of the AE energy exponent to details of sample morphology and the testing mode may be explained by the fact that the observed AE energy exponents β are close to the value $\beta = 1.5$, which is the exponent of the critical branching process, and hence the mean-field exponent for avalanche processes. This may be taken as one example of universal behavior that, while of academic interest, tends to be irrelevant in the context of materials science: what is universal cannot be changed, and hence cannot be subject to targeted design. What is nonuniversal, on the other hand, can be exploited—such as the artificial creation of structural hierarchy by targeted patterning that, as our findings demonstrate, may provide an efficient means of enhancing flaw tolerance of quasibrittle materials.

The idea of using cut patterns to improve mechanical properties has also been investigated in the context of enhancing stretchability of membrane sheets. Patterns of parallel cuts that are loaded in tension perpendicular to the cut direction (i.e., orthogonal to the direction investigated in the present study) give rise to complex, Kirigami-like out-of-plane deformation patterns. Machine learning techniques have been used to optimize such cut patterns in view of enhanced stretchability of sheetlike materials [39]. It may be a promising subject of future

studies to investigate whether hierarchical cut patterns might have any beneficial properties when loaded in the cut-perpendicular direction.

ACKNOWLEDGMENTS

M.P., S.A.H., and M.Z acknowledge support from the DFG, under grant No. Za171/9-3. M.A. and T.M. acknowledge support from the Academy of Finland (Center of Excellence program, 278367 and 317464), FinnCERES flagship (151830423), Business Finland (211835 and 211909), and Future Makers programs.

APPENDIX: EFFECT OF THE NUMBER OF HIERARCHY LEVELS

In a study by Mirzaeifar *et al.* [17], it was reported that the effect of hierarchical composite structure on defect tolerance may depend on the number of hierarchy levels. In order to assess whether such behavior may also be found for hierarchical gap patterns as investigated here, we performed simulations of 2D beam network models of quasibrittle sheets as described in Ref. [12]. In these simulations, DHP-type gap patterns with the same value of w_s and the same system size $L = 2^n = 256w_s$ (i.e., a maximum number of $n = 9$ hierarchy levels) were considered. Alongside the case $n = 9$, where the hierarchical pattern fills the entire sample, we also simulated gap patterns with a smaller number of hierarchy levels. To this end, a pattern with $n < 9$ of size $\xi = 2^{n-1}w_s$ was constructed, as described in the main paper (see Fig. 1), and then this pattern was periodically repeated in both load-parallel and load-perpendicular directions so as to fill the sample of edge length L . For these patterns, the periodicity length ξ defines an upper correlation length (“RVE size” in mechanics lingo) for the pattern with truncated hierarchical structure. We note that the case $n = 1$ corresponds to an unpatterned sheet (“NP sample” in the main paper).

Simulations were performed for both un-notched structures and for structures with a load-perpendicular side notch of length a with $0 \leq a \leq 0.8L$. As in the experiments, the notches were vertically located at random positions between 0.25 and 0.75 of the sample length in the loading direction. For each pair of values (a, n) , ten

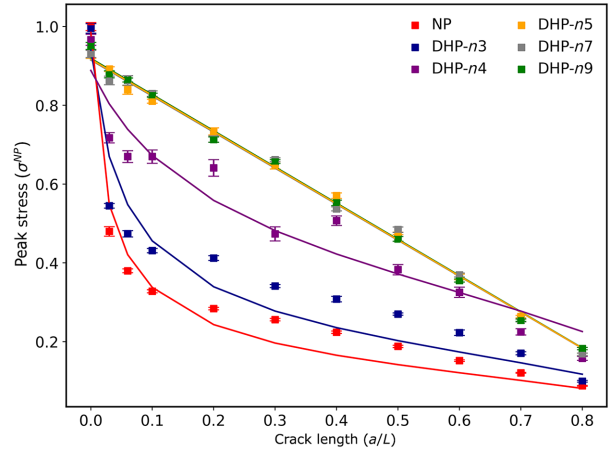


FIG. 11. Peak stress as a function of the notch length for DHP samples with different numbers of hierarchy levels between $n = 1$ (NP) and $n = 9$ (DHP-n9). All stresses are given in units of the mean peak stress σ^{NP} of an unpatterned and un-notched sample. The solid lines represent fit curves using Eq. (3) ($n \leq 4$) or Eq. (4) ($n \geq 5$).

simulations were performed to ensure statistical reliability of the results.

The results are shown in Fig. 11. With an increasing number of hierarchy levels, the failure stress of precracked samples increases monotonically for all investigated values of the crack length a . This increase saturates for $n \geq 5$, where a further increase in the number of hierarchy levels does not lead to appreciable further improvement in strength. To understand the reasons for this behavior, we have fitted the strength versus crack length curves using both Eq. (3), representing the expected behavior according to quasibrittle fracture mechanics, and Eq. (4), which represents the behavior we find to be typical of hierarchical materials. The best fit as measured by the value of R^2 is obtained for $n < 5$ by Eq. (3), whereas, for $n \geq 5$, the data are almost perfectly represented by Eq. (4). As can be seen from the fit parameters in Table II, the crossover occurs once the upper correlation length ξ of the hierarchical pattern significantly exceeds the process zone size of the unpatterned material.

Applying the criterion $\xi \gg a_0^{\text{NP}}$ to the experimental data on paper sheets in the main manuscript, we see that, for

TABLE II. Summary of fitting parameters for samples with different numbers of hierarchy levels, using Eqs. (3) and (4). The correlation length corresponding to a given hierarchy level is also included.

Sample	ξ (L)	R^2 [Eq. (3)]	a_0 (L)	K_{Ic} ($\sigma^{\text{NP}}\sqrt{L}$)	R^2 [Eq. (4)]	$\sigma_{(P,0)}$ (σ^{NP})
DHP-N9	1	0.95	0.1766	0.73	0.99	0.919
DHP-N7	0.250	0.94	0.1873	0.74	0.99	0.915
DHP-N5	0.0625	0.94	0.1889	0.75	0.99	0.916
DHP-N4	0.0312	0.93	0.1350	0.58	0.91	0.78
DHP-N3	0.0156	0.91	0.0309	0.29	0.66	0.60
NP	...	0.97	0.0133	0.20	0.52	0.50

the values of w_s used in our study and with the value of $a_0^{\text{NP}} = 31$ mm taken from Table I, this criterion is approximately fulfilled if $n > 5$, which is true for all hierarchically patterned samples in our study. For smaller values of n , a deterioration of flaw tolerance and a crossover towards the behavior of nonhierarchical NP and RP patterns is expected.

-
- [1] M. Alava and K. Niskanen, The physics of paper, *Rep. Prog. Phys.* **69**, 669 (2006).
- [2] J. Sun and B. Bhushan, Hierarchical structure and mechanical properties of nacre: A review, *RSC Adv.* **2**, 7617 (2012).
- [3] D. Jiao, Z. Liu, Z. Zhang, and Z. Zhang, Intrinsic hierarchical structural imperfections in a natural ceramic of bivalve shell with distinctly graded properties, *Sci. Rep.* **5**, 1 (2015).
- [4] H. Gao, Application of fracture mechanics concepts to hierarchical biomechanics of bone and bone-like materials, *Int. J. Fract.* **138**, 101 (2006).
- [5] J.-Y. Rho, L. Kuhn-Spearing, and P. Zioupos, Mechanical properties and the hierarchical structure of bone, *Med. Eng. Phys.* **20**, 92 (1998).
- [6] A. Gautieri, S. Vesentini, A. Redaelli, and M. J. Buehler, Hierarchical structure and nanomechanics of collagen microfibrils from the atomistic scale up, *Nano Lett.* **11**, 757 (2011).
- [7] D. Sen and M. J. Buehler, Structural hierarchies define toughness and defect-tolerance despite simple and mechanically inferior brittle building blocks, *Sci. Rep.* **1**, 1 (2011).
- [8] R. Oftadeh, B. Haghpanah, D. Vella, A. Boudaoud, and A. Vaziri, Optimal Fractal-Like Hierarchical Honeycombs, *Phys. Rev. Lett.* **113**, 104301 (2014).
- [9] S. Biswas and M. Zaiser, Avalanche dynamics in hierarchical fiber bundles, *Phys. Rev. E* **100**, 022133 (2019).
- [10] P. Moretti, B. Dietemann, N. Esfandiary, and M. Zaiser, Avalanche precursors of failure in hierarchical fuse networks, *Sci. Rep.* **8**, 1 (2018).
- [11] N. Esfandiary, M. Zaiser, and P. Moretti, Statistical aspects of interface adhesion and detachment of hierarchically patterned structures, *J. Stat. Mech.: Theory Exp.* **2022**, 023301 (2022).
- [12] S. A. Hosseini, P. Moretti, D. Konstantinidis, and M. Zaiser, Beam network model for fracture of materials with hierarchical microstructure, *Int. J. Fract.* **227**, 243 (2021).
- [13] S. A. Hosseini, P. Moretti, and M. Zaiser, Enhanced fault tolerance in biomimetic hierarchical materials: A simulation study, *Phys. Rev. Mater.* **7**, 053612 (2023).
- [14] M. Zaiser, S. A. Hosseini, P. Moretti, T. Mäkinen, J. Koivisto, M. Pournajar, M. Himmler, M. Redel, D. W. Schubert, and M. J. Alava, Hierarchical Slice Patterns Inhibit Crack Propagation in Brittle Sheets, *Phys. Rev. Appl.* **18**, 044035 (2022).
- [15] M. M. Driscoll, B. G.-g. Chen, T. H. Beuman, S. Ulrich, S. R. Nagel, and V. Vitelli, The role of rigidity in controlling material failure, *Proc. Natl. Acad. Sci.* **113**, 10813 (2016).
- [16] D. Bonamy and E. Bouchaud, Failure of heterogeneous materials: A dynamic phase transition?, *Phys. Rep.* **498**, 1 (2011).
- [17] R. Mirzaeifar, L. S. Dimas, Z. Qin, and M. J. Buehler, Defect-tolerant bioinspired hierarchical composites: Simulation and experiment, *ACS Biomater. Sci. Eng.* **1**, 295 (2015).
- [18] F. Hild and S. Roux, Digital image correlation: from displacement measurement to identification of elastic properties—a review, *Strain* **42**, 69 (2006).
- [19] J. Blaber, B. Adair, and A. Antoniou, Ncorr: Open-source 2D digital image correlation Matlab software, *Exp. Mech.* **55**, 1105 (2015).
- [20] M. Mustalahti, J. Rosti, J. Koivisto, and M. J. Alava, Relaxation of creep strain in paper, *J. Stat. Mech.: Theory Exp.* **2010**, P07019 (2010).
- [21] B. Pan, Reliability-guided digital image correlation for image deformation measurement, *Appl. Opt.* **48**, 1535 (2009).
- [22] L. Salminen, A. Tolvanen, and M. J. Alava, Acoustic Emission from Paper Fracture, *Phys. Rev. Lett.* **89**, 185503 (2002).
- [23] J. P. Sethna, K. A. Dahmen, and C. R. Myers, Crackling noise, *Nature* **410**, 242 (2001).
- [24] J. Baró and E. Vives, Analysis of power-law exponents by maximum-likelihood maps, *Phys. Rev. E* **85**, 066121 (2012).
- [25] M. Reichler, S. Rabensteiner, L. Törnblom, S. Coffeng, L. Viitanen, L. Jannuzzi, T. Mäkinen, J. R. Mac Intyre, J. Koivisto, and A. Puisto, *et al.*, Scalable method for bio-based solid foams that mimic wood, *Sci. Rep.* **11**, 1 (2021).
- [26] A. Miksic, J. Koivisto, J. Rosti, and M. Alava, Strain fluctuations from DIC technique applied on paper under fatigue or creep, *Procedia Eng.* **10**, 2678 (2011).
- [27] J. Rosti, J. Koivisto, and M. J. Alava, Statistics of acoustic emission in paper fracture: Precursors and criticality, *J. Stat. Mech.: Theory Exp.* **2010**, P02016 (2010).
- [28] Z. P. Bažant, Size effect in blunt fracture: Concrete, rock, metal, *J. Eng. Mech.* **110**, 518 (1984).
- [29] H. Tada, P. C. Paris, and G. R. Irwin, The stress analysis of cracks, Handbook, Del Research Corporation (ASME Press, 1973).
- [30] M. J. Alava, P. K. Nukala, and S. Zapperi, Role of Disorder in the Size Scaling of Material Strength, *Phys. Rev. Lett.* **100**, 055502 (2008).
- [31] M. J. Alava, P. K. Nukala, and S. Zapperi, Statistical models of fracture, *Adv. Phys.* **55**, 349 (2006).
- [32] J. Koivisto, M. Ovaska, A. Miksic, L. Laurson, and M. J. Alava, Predicting sample lifetimes in creep fracture of heterogeneous materials, *Phys. Rev. E* **94**, 023002 (2016).
- [33] J. Rosti, J. Koivisto, L. Laurson, and M. J. Alava, Fluctuations and Scaling in Creep Deformation, *Phys. Rev. Lett.* **105**, 100601 (2010).
- [34] F. Louchet and P. Duval, Andrade creep revisited, *Int. J. Mater. Res.* **100**, 1433 (2009).
- [35] H. Nechad, A. Helmstetter, R. El Guerjouma, and D. Sornette, Creep Ruptures in Heterogeneous Materials, *Phys. Rev. Lett.* **94**, 045501 (2005).
- [36] L. Viitanen, M. Ovaska, S. K. Ram, M. J. Alava, and P. Karppinen, Predicting Creep Failure from Cracks in a Heterogeneous Material Using Acoustic Emission

- and Speckle Imaging, [Phys. Rev. Appl. **11**, 024014 \(2019\)](#).
- [37] H. Gao, in *Advances in Fracture Research: Honour and Plenary Lectures Presented at the 11 th International Conference on Fracture (ICF11), Held in Turin, Italy, on March 20–25, 2005* (Springer, 2006), p. 101.
- [38] H. Yao and H. Gao, Multi-scale cohesive laws in hierarchical materials, [Int. J. Solids Struct. **44**, 8177 \(2007\)](#).
- [39] P. Z. Hanakata, E. D. Cubuk, D. K. Campbell, and H. S. Park, Accelerated Search and Design of Stretchable Graphene Kirigami Using Machine Learning, [Phys. Rev. Lett. **121**, 255304 \(2018\)](#).